ADVANCED MATERIALS
www.advmat.de

Ultrathin, Cationic Covalent Organic Nanosheets for Enhanced CO_2 Electroreduction to Methanol

Yun Song, Peng Guo, Tinghao Ma, Jianjun Su, Libei Huang, Weihua Guo, Yong Liu, Geng Li, Yinger Xin, Qiang Zhang, Siwei Zhang, Hanchen Shen, Xing Feng, Dengtao Yang, Jia Tian, Sai Kishore Ravi, Ben Zhong Tang, and Ruquan Ye**

Metalloporphyrins and metallophthalocyanines emerge as popular building blocks to develop covalent organic nanosheets (CONs) for CO_2 reduction reaction (CO_2RR). However, existing CONs predominantly yield CO, posing a challenge in achieving efficient methanol production through multielectron reduction. Here, ultrathin, cationic, and cobalt-phthalocyanine-based CONs (iminium-CONs) are reported for electrochemical CO_2-to-CH_3OH conversion. The integration of quaternary iminium groups enables the formation of ultrathin morphology with uniformly anchored cobalt active sites, which are pivotal for facilitating rapid multielectron transfer. Moreover, the cationic iminium-CONs exhibit a lower activity for hydrogen evolution side reaction. Consequently, iminium-CONs manifest significantly enhanced selectivity for methanol production, as evidenced by a remarkable 711% and 270% improvement in methanol partial current density (j_{CH3OH}) compared to pristine CoTAPc and neutral imine-CONs, respectively. Under optimized conditions, iminium-CONs deliver a high j_{CH3OH} of 91.7 mA cm^{-2} at −0.78 V in a flow cell. Further, iminium-CONs achieve a global methanol Faradaic efficiency (FE_{CH3OH}) of 54% in a tandem device. Thanks to the single-site feature, the methanol is produced without the concurrent generation of other liquid byproducts. This work underscores the potential of cationic covalent organic nanosheets as a compelling platform for electrochemical six-electron reduction of CO_2 to methanol.

1. Introduction

The excessive consumption of fossil fuels and the subsequent substantial CO_2 emissions have unequivocally been identified as the primary drivers of the global energy and environmental crisis.[1–3] Electrocatalytic reduction of CO_2 into fuels using renewable energy has emerged as a sustainable solution to these problems.[4–7] However, the intrinsic chemical inertia of CO_2 and the competitive hydrogen evolution reaction (HER) often impede the achievement of high energy efficiency and selectivity.[8] Consequently, extensive efforts have been dedicated to developing efficient electrocatalysts with high product selectivity and durability. Various catalysts, including metal alloys,[9,10] metal oxides,[11,12] single-atom materials,[13,14] and metal–organic complexes,[15,16] have been investigated. Notably, molecular catalysts[17] such as metalloporphyrins[18] and metallophthalocyanines[19] have gathered substantial attention due to their tailorable catalytic efficiency and product selectivity, which can be rationally regulated via the electronic effects of the ligands.

Y. Song, J. Su, L. Huang, W. Guo, Y. Liu, G. Li, Y. Xin, Q. Zhang, R. Ye
Department of Chemistry and State Key Laboratory of Marine Pollution
City University of Hong Kong
Hong Kong 999077, China
E-mail: ruquanye@cityu.edu.hk

P. Guo, J. Tian
Key Laboratory of Synthetic and Self-Assembly Chemistry for Organic Functional Molecules
Center for Excellence in Molecular Synthesis
Shanghai Institute of Organic Chemistry
University of Chinese Academy of Sciences
Chinese Academy of Sciences
345 Lingling Road, Shanghai 200032, China
E-mail: tianjia@sioc.ac.cn

T. Ma, D. Yang
School of Chemistry and Chemical Engineering
Northwestern Polytechnical University
Xi'an 710072, China

S. Zhang, H. Shen, B. Z. Tang
Shenzhen Institute of Molecular Aggregate Science and Engineering
School of Science and Engineering
The Chinese University of Hong Kong
Longgang District
Shenzhen 518172, China

S. Zhang, H. Shen, B. Z. Tang
Department of Chemistry and the Hong Kong Branch of Chinese National Engineering Research Center for Tissue Restoration and Reconstruction
The Hong Kong University of Science and Technology
Hong Kong 999077, China

The ORCID identification number(s) for the author(s) of this article can be found under https://doi.org/10.1002/adma.202310037

DOI: 10.1002/adma.202310037

So far, a plethora of molecular catalysts featuring desirable functional groups have been designed and employed as effective electrocatalysts for CO_2 reduction reaction (CO_2RR), such as nickel tetrakis(methoxy)phthalocyanine,[20] iron tetra(p-*N,N,N*-trimethylanilinium)porphyrin,[21] and cobalt 5,10,15,20-tetrakis(4-(pyren-1-yl)phenyl)porphyrin.[22] The integration of molecular catalysts into covalent organic polymers is another strategy for designing effective CO_2RR electrocatalysts.[23–25] In this approach, molecular catalysts serve as uniformly isolated active sites within the covalent organic polymer framework.[6] Meanwhile, the electronic configuration of the active sites can be controlled by adjacent functional groups in the framework,[26] thereby offering opportunities to tailor the intrinsic catalytic performance of the catalysts.

Cobalt-based molecular catalysts and their integration into covalent organic polymers have been extensively investigated for CO_2RR.[27–29] However, the predominant product is CO, with only a few sporadic studies reporting the generation of deeply reduced products such as methanol.[30–32] In 2019, researchers demonstrated a hybrid catalyst comprising cobalt phthalocyanine immobilized on multiwalled carbon nanotube (CoPc/CNT) for CO_2-to-methanol conversion.[30,32] The CoPc/CNT delivered a methanol partial current density of 10.6 mA cm^{-2} and a high methanol Faradaic efficiency (FE_{CH3OH}) of 44%.[32] Wang et al. emphasized the critical importance of dispersing CoPc as individual molecules on conductive CNT supports to ensure rapid and uninterrupted electron transfer to the active sites for the six-electron reduction of CO_2. In contrast, the physical mixing of excessive CoPc with CNTs inevitably led to random dispersion and aggregation of CoPc molecules, severely hampering the selectivity and activity of methanol production. Despite the thrilling methanol selectivity of CoPc/CNT, the cobalt content was deliberately maintained at an extremely low concentration of ≈0.27% to preserve the monodisperse packing of CoPc on CNT, resulting in limited current density. In addition, CoPc/CNT exhibited a narrow potential window for efficient methanol production. The partial current density and FE of H_2 increased with overpotential and eventually dominated after −0.94 V versus RHE.

Inspired by the beneficial role of cationic surfactants in enhancing CO_2RR activity and suppressing HER activity;[33–37] here, we reported a positively charged ultrathin covalent organic nanosheet for electrocatalytic CO_2-to-methanol conversion. We first prepared imine-bridged covalent organic nanosheets (imine-CONs) from the polymerization of cobalt(II) 2,9,16,23-tetra(amino)phthalocyanine (CoTAPc) and 2,5-ditert-butyl-1,4-benzoquinone (DTBBQ), followed by post-synthetic modification of imine-CONs with methyl iodide to yield quaternized iminium-CONs. The steric hindrance imparted by the tert-butyl groups in DTBBQ units and the electrostatic repulsion effect of positively charged quaternary iminium groups assisted the formation of 2D ultrathin nanosheets. The resulting iminium-CONs exhibited highly exposed and atomically isolated cobalt active sites on the surface, enabling efficient electron transfer and promoting the generation of methanol when combined with conductive carbon substrates. At the same time, the positively charged framework of iminium-CONs inhibited the side hydrogen evolution reaction. Experimental results demonstrated that the iminium-CONs attained a FE_{CH3OH} of 43.4% with a partial current density of 7.8 mA cm^{-2} at −1 V in an H-cell and delivered a methanol partial current density of 90.3 mA cm^{-2} with FE_{CH3OH} of 38.7% at −0.74 V in a flow cell. The competitive HER was suppressed to 48.9% under high overpotential (−0.89 V vs RHE), outperforming Co-TAPc (73.5% at −0. 88 V vs RHE). We also investigated the activity of iminium-CONs toward carbon monoxide reduction reaction (CORR), yielding a global FE_{CH3OH} of 54%.

2. Results and Discussion

As shown in **Figure 1**a, imine-CONs were synthesized by the condensation reaction of CoTAPc and DTBBQ in 1:2 molar ratio in a mixed solvent of ethanol and *N,N*-dimethylacetamide for 72 h,[38] and a subsequent methylation to obtain iminium-CONs. To further highlight the significance of cationic nanosheet structure in reducing the hydrogen evolution reaction, the ionic molecular catalyst, cobalt(II) tetra-(4-*N,N,N*-trimethylanilinium)phthalocyanine (CoTMAPc), was also prepared by methylating CoTAPc. The chemical structure of the as-prepared samples was characterized by Fourier transform infrared (FT-IR) spectroscopy, Raman spectroscopy, ^{13}C solid-state nuclear magnetic resonance (^{13}C NMR) spectroscopy, and X-ray photoelectron spectroscopy (XPS). CoTAPc displays typical peaks of phthalocyanine moiety at 1705, 1607, 1491, 1334 1259, 825, and 751 cm^{-1}, and the peaks at 3324 and 3193 cm^{-1} were assigned to N—H stretching of amino groups (Figure 1b). For CoTMAPc, the peaks at 1484 and 940 cm^{-1} resulted from —CH_3 stretching and C—N^+ bending. The transformation of CoTAPc into CoTMAPc could also be verified by ^1H nuclear magnetic resonance (^1H NMR) spectroscopy. The prominent peak located at 3.14 ppm was attributed to the presence of methyl proton in CoTMAPc, indicating that the methylation modification was completed (Figure S1a, Supporting Information). The newly formed imine bond in the condensed imine-CONs exhibited a C=N stretching at 1641 cm^{-1}; while, the C−H stretching bands of tert–butyl group were observed at 2908 and 2852 cm^{-1}. The appearance of −CH_3 and C−N^+ vibration peaks at 1480 and 942 cm^{-1} and the retention of C=N vibration peak (1642 cm^{-1}) after the methylation reaction confirmed the formation of ionic covalent organic polymer, iminium-CONs. In the Raman spectra (Figure S1b, Supporting Information), CoTAPc and its derived catalysts all presented characteristic peaks in the range between 500 and 1600 cm^{-1}. The chemical structure of iminium-CONs was further determined by ^{13}C NMR. The ^{13}C NMR signals in Figure S1c, Supporting Information were broad due to the magnetic property of cobalt complex. CoTAPc presented peaks at 172.7, 144.6, 129, and 120.5 ppm, which could be assigned to

X. Feng
Guangdong Provincial Key Laboratory of Information Photonics Technology
School of Material and Energy
Guangdong University of Technology
Guangzhou 510006, P. R. China
S. K. Ravi
School of Energy and Environment
City University of Hong Kong
Hong Kong 999077, China
Y. Song, R. Ye
City University of Hong Kong Shenzhen Research Institute
Shenzhen 518057, China

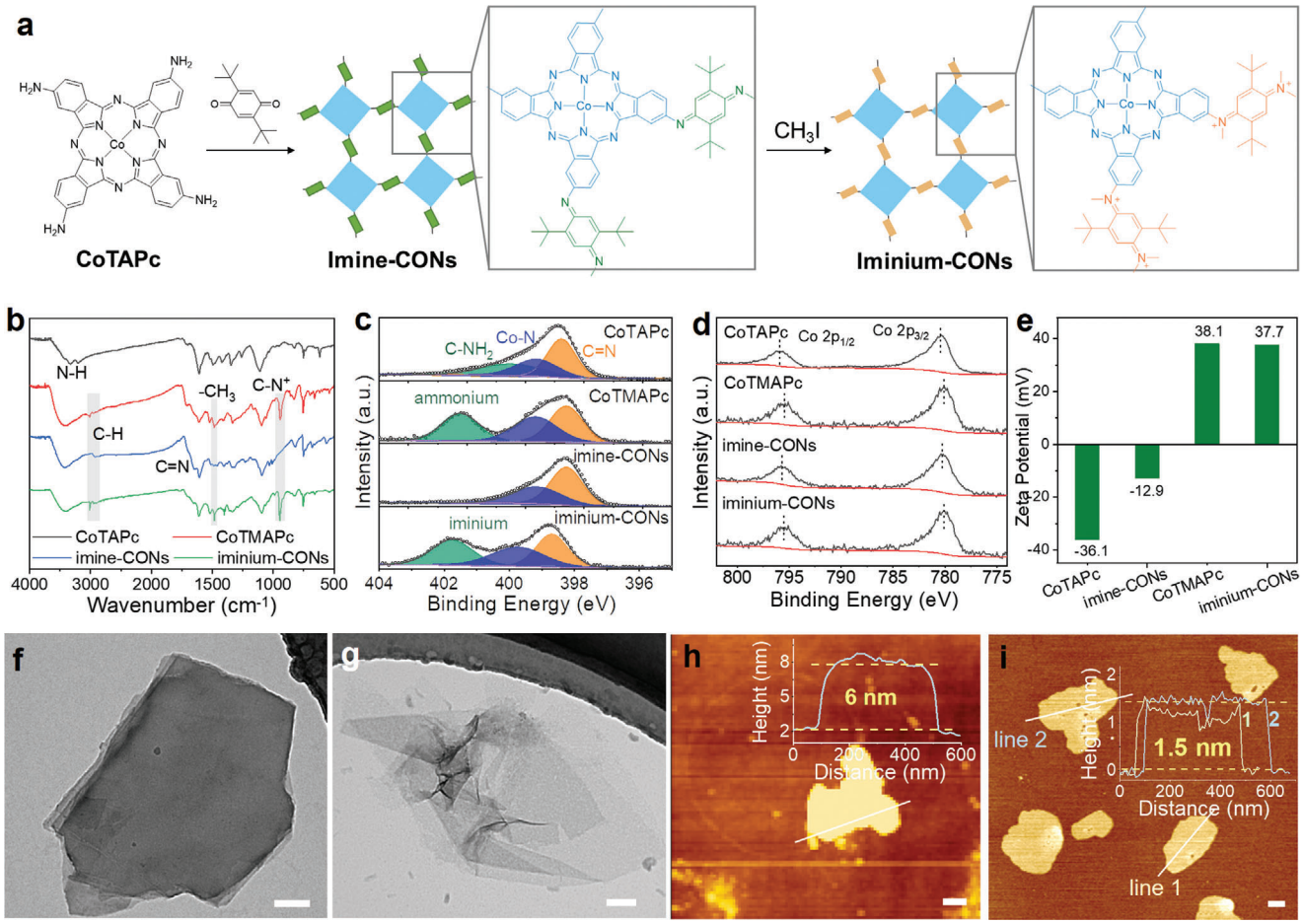

Figure 1. a) Schematic illustration for the synthesis of iminium-CONs. b) FT-IR spectra. c) N 1s XPS spectra. d) Co 2p XPS spectra. e) Zeta potential of CoTAPc, CoTMAPc, imine-CONs, and iminium-CONs. f,g) TEM images of imine-CONs and iminium-CONs. Scale bar: 100 nm. h,i) AFM images of imine-CONs and iminium-CONs. Scale bar: 100 nm.

the aromatic carbons of cobalt phthalocyanine. A sharp peak of CoTMAPc at 56.8 ppm corresponded to the methyl carbon. For imine-CONs, imine linkage formation was evident by the appearance of a signal at 146.6 ppm. Compared with imine-CONs, iminium-CONs showed a unique peak at 31.8 ppm, which was attributed to the methyl carbon of iminium unit.

XPS measurements are conducted to analyze the elemental compositions and surface valence states of covalent organic nanosheets. The N 1s spectrum for CoTAPc can be deconvoluted into amino N (400.4 eV), pyrrolic N (399.6 eV), and pyridinic N (398.8 eV). Iminium-CONs show similar peaks at 399.7 and 398.6 eV, corresponding to the pyrrolic N and pyridinic N of phthalocyanine ring. The new peak at 401.8 eV is ascribed to the quaternary N of iminium-CONs. The area ratio of iminium N, pyrrolic N, and pyridinic N is close to 1:1:1 for iminium-CONs, which indicates that the imine groups are fully turned into quaternary iminium groups. The quaternary ammonium peak of CoTMAPc is found at 402.2 eV, slightly higher than the iminium peak (401.8 eV) of iminium-CONs due to different chemical environments.[39,40] Figure 1d displays the Co 2p XPS spectra. The binding energies of Co $2p_{3/2}$ and Co $2p_{1/2}$ for CoTAPc are 795.8 and 780.4 eV. Compared with CoTAPc, the Co peaks of both CoTMAPc and iminium-CONs are shifted to lower energies due to the electron-withdrawing effect of quaternized nitrogen groups, which decrease the electron density of cobalt sites.[41,42] The optical property of iminium-CONs is characterized using UV–vis spectra in Figure S2, Supporting Information. Imine-CONs show a Q band at 699.8 nm, whereas the iminium-CONs show a blueshift at 667.6 nm for the electron withdrawing effect.[43,44] In addition, the cobalt contents of CoTAPc, CoTMAPc, imine-CONs, and iminium-CONs are determined to be 7.1%, 5.8%, 4.3%, and 4.1 wt% by ICP-OES. Zeta potential analysis is also applied to check the positively charged structure of iminium-CONs in Figure 1e. The ethanol suspensions of CoTAPc, imine-CONs, CoTMAPc, and iminium-CONs show zeta potential values of −36.1, −12.9, 38.1, and 37.7 mV, respectively (detailed distribution curves in Figure S3, Supporting Information). The morphologies of the covalent organic nanosheets are characterized by transmission electron microscopy (TEM) and atomic force microscopy (AFM). Imine-CONs are in the shape of few-layered nanosheets with a thickness of ≈6 nm. Iminium-CONs show well-preserved 2D nanosheet morphology with no apparent morphological changes after methylation; while, the thickness is reduced to ≈1.5 nm. Further, the corresponding

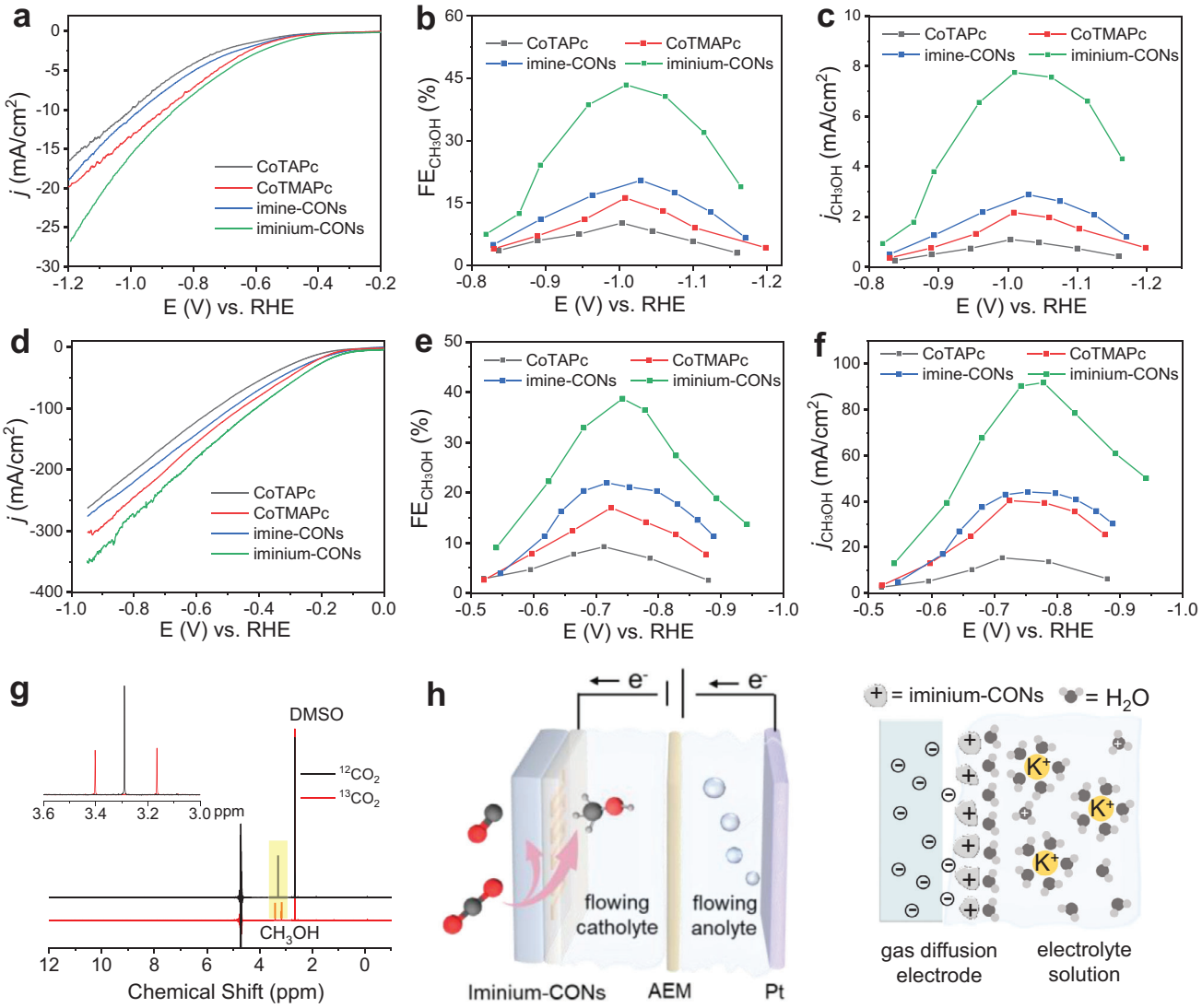

Figure 2. Electrocatalytic CO_2RR performance of molecular catalysts and covalent organic nanosheets. a) LSV curves, b) faradaic efficiency, and c) partial current density toward methanol of CoTAPc, CoTMAPc, imine-CONs, and iminium-CONs in a H-cell. d) LSV curves, e) faradaic efficiency, and f) partial current density toward methanol of CoTAPc, CoTMAPc, imine-CONs, and iminium-CONs using mixed electrolyte of 0.2 M KOH and 1.5 M KCl in a flow cell. Error bars present the standard deviation of three independent measurements. g) ^{1}H NMR spectra of methanol product of iminium-CONs catalyst in $^{12}CO_2$ and $^{13}CO_2$ saturated solutions. h) Schematic of electrochemical flow cell and interfacial ions on the catalyst surface.

element mapping analysis is shown in Figure S4, Supporting Information; Co, N, I, and C elements are evenly distributed over the entire framework of iminium-CONs. The powder X-ray diffraction (XRD) pattern illustrates the amorphous nature of covalent organic nanosheets due to less symmetry of CoTAPc. In Figure S1d, Supporting Information, imine-CONs exhibit a broad diffraction peak at 26.3°; while, the diffraction peak of iminium-CONs shifts to 20.9° with decreasing CON thickness. These results verify that iminium-CONs possess the structure of positively charged ultrathin nanosheets with uniformly distributed cobalt active sites, which is critical for the electrocatalytic reduction of CO_2 into methanol, as discussed below.

The electrocatalytic performance of all catalysts is first tested in an H-cell using CO_2-saturated 0.5 M $KHCO_3$ electrolyte. The loading content of cobalt in different catalysts is kept consistent by controlling the catalyst amount. Linear sweep voltammetry (LSV) polarization curves are presented in **Figure 2**a. Iminium-CONs show a more positive onset potential (−0.37 V) and higher current density than other samples at the applied potential range from −0.4 to −1.2 V versus RHE. This trend is similar to our previous report of ultrathin, cationic porphyrin-based CONs.[23] The products of CO_2RR at each potential are further investigated in chronoamperometry experiments (Figures S5 and S6, Supporting Information). The generated gas and liquid products are analyzed by online gas chromatograph (GC) and ^{1}H nuclear magnetic resonance spectroscopy, with CO, H_2, and CH_3OH detected as the main products. It can be seen from Figure 2b that the methanol production of iminium-CONs occurs at −0.82

V versus RHE. The methanol selectivity of iminium-CONs increases with larger overpotential and achieves a maximum value of 43.4% at −1 V, a 212% and 268% improvement compared with imine-CONs (20.5% at −1.03V) and CoTMAPc (16.2% at −1 V). In contrast, the CoTAPc electrode, which contains the same cobalt content as iminium-CONs, shows an inferior electrochemical performance with lower current density and FE_{CH3OH}. Even at a higher potential of −1.16 V, iminium-CONs still maintain a moderate FE_{CH3OH} of 18.9% and FE_{H2} of 57.7%, superior to CoTAPc with 70.4% FE_{H2}. In addition, iminium-CONs show the highest j_{CH3OH} at the potential range from −0.82 to −1.16 V (Figure 2c). To further determine the source of CH_3OH, the ^{13}C-labeling CO_2 isotope experiment is carried out. Figure 2g displays the characteristic doublet $^{13}CH_3OH$ at 3.4 and 3.16 ppm, indicating that methanol originates from the reduction of CO_2. Controlled experiments performed under argon atmosphere further support that the methanol is produced by CO_2 reduction other than an impurity (Figure S9, Supporting Information).

Considering that the current density in H-type cell is restricted by mass transport due to the low solubility of CO_2, the electrocatalytic CO_2RR performance is further evaluated in a flow cell reactor. As revealed by Robert, formaldehyde, an important intermediate of electrochemical conversion of CO_2 to CH_3OH, is not available at pH above 14 because its hydrated form of methylene glycol has a pKa of ≈13 and is mostly deprotonated at pH 14.[30] Therefore, here we use a mixed electrolyte of 0.2 M KOH and 1.5 M KCl. Figure 2h presents the schematic illustration of the electrocatalytic flow cell configuration and the catalytic interface of iminium-CONs cathode. The onset potential of iminium-CONs positively shifts to −0.11 V, and the current density reaches 350 mA cm^{-2} at −0.95 V in Figure 2d. Iminium-CONs deliver a high partial current density of 90.3 mA cm^{-2} at −0.74 V, and the FE_{CH3OH}, $FE_{CO,}$ and FE_{H2} are 38.7%, 39.3%, and 22%, respectively. In comparison, the partial current density of methanol on unmodified imine-CONs sample decreases to 43 mA cm^{-2} at −0.72 V with FE_{CH3OH}, $FE_{CO,}$ and FE_{H2} of 21.9%, 46.6%, and 31.5%, respectively. These results reveal that decorating CONs with cationic functional groups not only improves its electrocatalytic activity and selectivity to methanol but also suppresses the competitive HER. A similar phenomenon can be observed from CoTAPc and CoTMAPc in Figure 2e,f. CoTAPc yields a lower j_{CH3OH} of 15.4 mA cm^{-2} and lower FE_{CH3OH} of 9.2% at −0.71 V than that of CoTMAPc (40.4 mA cm^{-2} and 17% at −0.72V). However, CoTMAPc suffers from significant current decay due to the instinct water solubility of ionic molecular catalysts. Implanting the ionic moieties into the extended skeleton of covalent organic nanosheets can effectively mitigate the leaching problem. Moreover, the positively charged iminium-CONs would provide a platform for good dispersion and ideal exposure of catalytic cobalt active sites. The electrochemical active surface areas (ECSA) of obtained catalysts are determined by their electrochemical double-layer capacitances (C_{dl}, Figure S10, Supporting Information). The ECSA for iminium-CONs is calculated as 25.9 mF cm^{-2}, higher than that of CoTAPc (9.6 mF cm^{-2}), CoTMAPc (11.6 mF cm^{-2}), and imine-CONs (15.3 mF cm^{-2}). It indicates that the ultrathin iminium-CONs can provide more accessible surface in the electrocatalytic process. Electrochemical impedance spectroscopy (EIS) tests are conducted to reveal the electrocatalytic kinetics on the electrode/electrolyte surface during CO_2RR (Figure S11, Supporting Information). Nyquist plots show that the charge transfer resistance of iminium-CONs (2.3 Ω) is smaller than that of CoTAPc (4.9 Ω), CoTMAPc (3.7 Ω), and imine-CONs (4.1 Ω), which indicates faster electron transfer of electrocatalytic CO_2-to-methanol conversion for iminium-CONs. Iminium-CONs(BF_4) are synthesized via anion exchange by substituting I^- with BF_4^- to investigate whether iodide ions affect the performance of CO_2RR. As shown in Figure S12, Supporting Information, methanol production starts at −0.54 V and reaches a maximum FE of 38.5% at −0.75 V. The current density and Faradic efficiency of iminium-CONs(BF_4) are similar to those of iminium-CONs, suggesting the minor contributions from anions.

As CO is the intermediate for electroreduction of CO_2 into CH_3OH and the efficiency of CO_2-to-CO selectivity has achieved nearly 100%,[17,30,34,45] we then explored the methanol generation using CO as the starting reactant. The electrocatalytic carbon monoxide reduction reaction (CORR) was first evaluated in a home-made H-cell using 0.5 M K_2SO_4 as the electrolyte. Iminium-CONs exhibited an onset potential of −0.56 V and a high current density of 28.8 mA cm^{-2} at −1.1 V in CO-saturated electrolyte (**Figure 3**a). Figure 3b shows that iminium-CONs displayed a higher FE_{CH3OH} than the other two counterparts. Notably, the FE_{CH3OH} of iminium-CONs reached 46.2% at −0.94 V; whereas, the methanol faradic efficiencies of pristine CoTAPc and imine-CONs were 9.2% and 18.8%, respectively. In addition, the partial current densities were calculated and are shown in Figure 3c. The highest CH_3OH partial current density of iminium-CONs was up to 4 mA cm^{-2} at −0.94 V, which was 7.69 and 2.72 times higher than that of CoTAPc and imine-CONs. The CORR was also applied in a flow cell. The FE_{CH3OH} of iminium-CONs increased with higher overpotential, from 14.3% at −0.54 V to a maximum of 44.1% at −0.87 V and declined to 22% at −1.07 V (Figure 3e). A global FE of 54% was calculated for the tandem reaction based on the CO_2-to-CO conversion with an FE of 98% (Figure S19, Supporting Information). Further, iminium-CONs exhibited a maximum methanol partial current density of 75.1 mA cm^{-2} at −0.94 V, much higher than that of neutral imine-CONs (31.2 mA cm^{-2} at −0.92 V). We then measured the HER of the catalysts in 0.5 M K_2SO_4 electrolyte (pH=2) using rotating disk electrode (RDE) under N_2 atmosphere.[46] Iminium-CONs showed a more negative onset potential and lower current density in the potential range from −0.4 to −1.17 V for the HER. A current density plateau of 140 mA $cm-^2$ was observed, and hydronium ions were depleted with further increases in current density (Figure S20, Supporting Information). The above results suggest that the steric hindrance and electrostatic repulsion effect made the positively charged iminium-CONs uniformly dispersed and the cobalt active sites highly exposed. On the other hand, the iminium unit synergistically inhibited the competing HER by electrostatic repulsion between cationic iminium moieties and protons, thereby benefiting the six-electron reduction of CO_2 to methanol.

We further studied the electrochemical stability of iminium-CONs toward CO_2RR and CORR in a flow cell electrolyzer (**Figure 4**a,b). The current density of CO_2RR maintained ≈215.5 mA cm^{-2} at −0.74 V for 6 h with a stable FE_{CH3OH} of 36.2%. XPS and UV–vis characterizations were carried out after electrolysis (Figure S21, Supporting Information). The Co 2p peaks

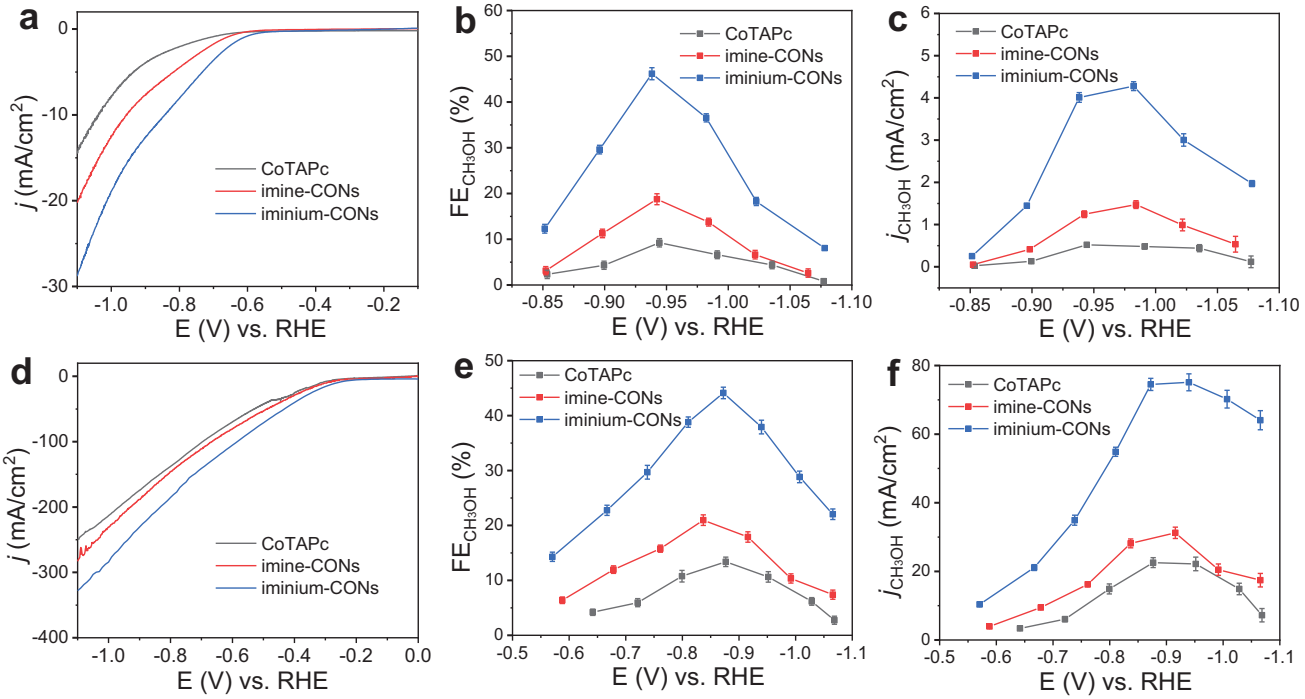

Figure 3. Electrocatalytic CORR performance of CoTAPc and covalent organic nanosheets. a) LSV curves in CO-saturated 0.5 M K_2SO_4, b) faradaic efficiency, and c) partial current density toward methanol of CoTAPc, imine-CONs, and iminium-CONs in a H-cell. d) LSV curves, e) faradaic efficiency, and f) partial current density toward methanol of CoTAPc, imine-CONs, and iminium-CONs using mixed electrolyte of 0.2 M KOH and 1.5 M KCl in a flow cell. Error bars present the standard deviation of three independent measurements.

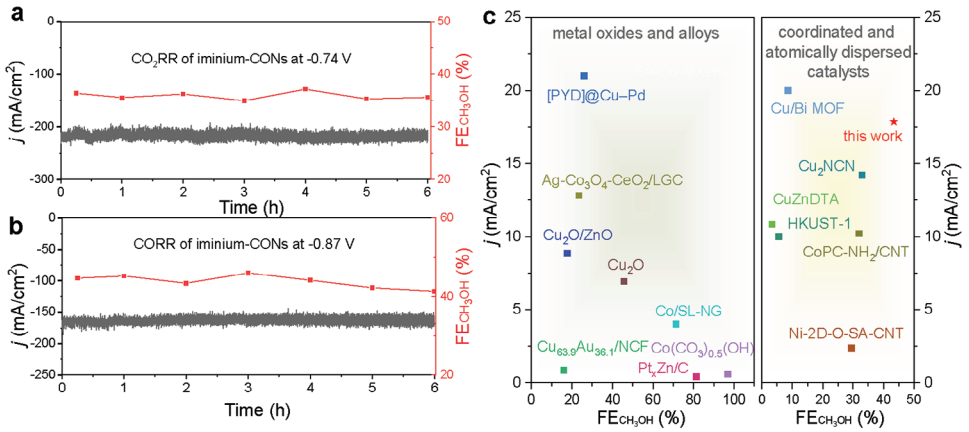

Figure 4. a,b) Stability test of iminium-CONs toward CO_2RR and CORR in a flow cell. c) Comparison of our results with previous data in terms of current density and faradaic efficiency.

revealed no obvious changes after the stability test, indicating the Co metal center preserves its primary valence state of +2. Meanwhile, the UV–vis spectra of iminium-CONs were almost the same before and after CO_2RR, suggesting the structure of iminium-CONs was retained during the stability tests. The crystal structure of iminium-CONs coated on gas diffusion layer electrode after long-term electrolysis was further analyzed, and two diffraction peaks at 17.9° and 25.8° were observed from Figure S21c, Supporting Information, which were indexed to the commercial GDL electrode. No peaks of cobalt oxide or cobalt metal were detected after electrolysis, suggesting that no dementalization occurred. The long-term electrolysis of carbon monoxide was performed at −0.87 V, with no significant decay of the current density and FE_{CH3OH}. Finally, we summarized the recently reported electrocatalysts,[47–55] including metal oxides and metal alloys, for electrocatalytic CO_2-to-CH_3OH conversion (Figure 4c). For a reasonable comparison, we only included data in aqueous electrolytes using H-cell. Iminium-CONs delivered a partial current density of 7.8 mA cm^{-2} with FE_{CH3OH} of 43.4% at −1 V, outperforming most coordinated and atomically-dispersed

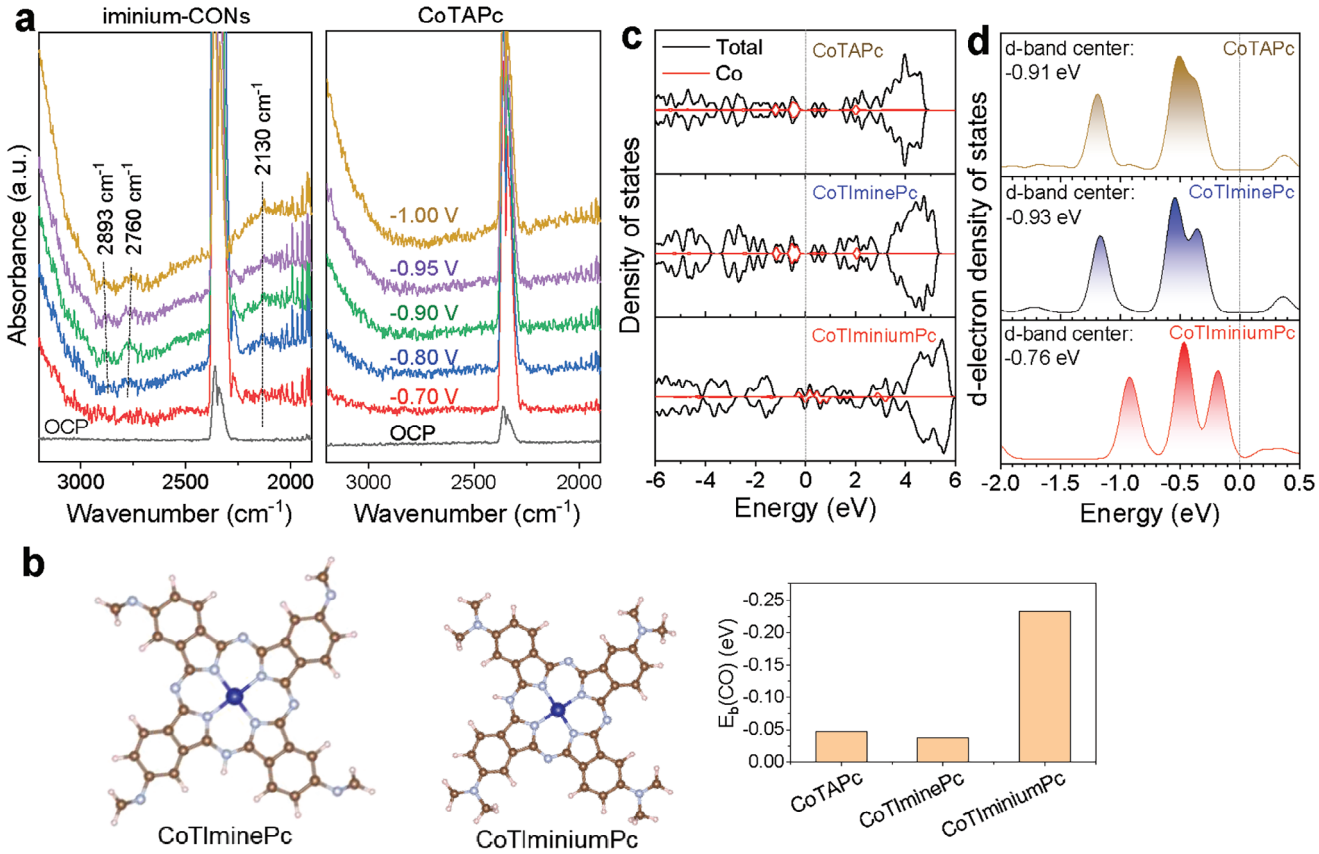

Figure 5. a) In situ attenuated total reflectance-surface enhanced infrared absorption spectroscopy of iminium-CONs and CoTAPc in CO_2-saturated 0.5 M $KHCO_3$ solution. b) Model of CoTImminePc, CoTIminiumPc, and the CO binding energy for different models. The calculated c) density of states (DOS) and d) Co d-electron DOS of CoTAPc, CoTImminePc, and CoTIminiumPc. The dashed line indicates Fermi level.

catalysts.[32,56–60] Our performance also surpasses many metal-based catalysts, which typically yield a mixture of liquid products.

To unravel the mechanism of methanol production, in situ attenuated total reflectance-surface enhanced infrared absorption spectroscopy (ATR-SEIRAS) measurements and DFT calculations were performed. **Figure 5**a presents the potential-dependent in situ ATR-SEIRAS spectra using iminium-CONs as the catalyst in CO_2 saturated 0.5 M $KHCO_3$ electrolyte. The peak around 2130 cm^{-1} appeared at −0.7 V and could be assigned to the adsorption of CO on iminium-CONs surface, which was a crucial intermediate of methanol generation. At higher overpotentials, new peaks at 2760 and 2893 cm^{-1} were observed, corresponding to the intermediate of *CHO and *CH_XO. The in situ ATR-SEIRAS data hints at the following mechanism of methanol production: CO_2 is first adsorbed to generate *COOH intermediate. After *COOH is formed, it can be reduced to obtain *CO species. Subsequently, a proton-coupled electron transfer process occurs at the cobalt active site to form *CHO intermediate, which is then reduced to methanol. This pathway aligns with recent literatures.[30,61,62] On the contrary, the ATR-SEIRAS spectra obtained from the CoTAPc surface (Figure 5a) shows no obvious *CO stretching vibration between 1800 and 2200 cm−^{1} and C—H between 2600 and 3000 cm−^{1}, indicating the low surface coverage of important intermediates for methanol production; so that, CO is the primary reduction product.

To further delve into the effect of peripheral functionalities, density functional theory calculations were performed. As the calculation for periodic materials was not suitable for slabs carrying charges;[21] here, we used the simplified models as shown in Figure 5b; Table S1, Supporting Information to account for the quaternary ammonium groups. Three different model molecules with peripheral functional groups of amine (CoTAPc), imine (CoTImminePc), and iminium (CoTIminiumPc) were used to represent CoTAPc, imine-CONs, and iminium-CONs, respectively, with a similar intermediate to our recent publication.[62] As the reduction of CO_2 to methanol was hindered by the weak adsorption to the intermediate *CO,[32,62] most of the molecular catalysts favored the desorption of CO and produced CO as the major product. A stronger binding to the *CO would be important to its further reduction. The binding energy is defined as

$$E_b\,(\mathrm{CO}) = E\,(*\,\mathrm{CO}) - E\,(*) - E\,(\mathrm{CO}) \quad (1)$$

where * denotes the cobalt site. The E_b(CO) for CoTAPc, CoTImminePc, and CoTIminiumPc were −0.047, −0.037, and −0.233 eV, respectively, indicating the most favorable CO adsorption at CoTIminiumPc. This can also be inferred from the shorter Co—C_{CO} distance of 1.84 Å for CoTIminiumPc than CoTAPc at 2.37 Å. We also compared the energy for the first-step hydrogenation of *CO to form *CHO (Figure S22, Supporting Information),

showing a similar energy barrier with slightly more favorable at the CoTIminiumPc. Our calculation showed that quaternary ammonium groups could enhance the *CO adsorption; thus, benefiting the further reduction to produce methanol. The calculation was consistent with the ATR-SEIRAS results.

To further understand how the peripheral functional groups change the electronic structures of the catalysts, the density of states (DOS) and Co d-band center energy levels of CoTAPc, CoTIminePc, and CoTlminiumPc were computed. Compared to CoTAPc and CoTIminePc, CoTlminiumPc manifested a significant shift in electronic structure (Figure 5c). The d-band centers energy levels of CoTAPc, CoTIminePc, and CoTlminiumPc were calculated to be −0.91, −0.93, and −0.76 eV (Figure 5d), suggesting that CoTlminiumPc has the strongest absorption ability. These results were consistent with the CO binding energy calculated in Figure 5b.

3. Conclusion

In summary, we have successfully synthesized a cobalt–phthalocyanine-based electrocatalyst in the form of positively charged covalent organic nanosheets (iminium-CONs) for CO_2-to-CH_3OH conversion. The incorporation of quaternary iminium groups facilitates the generation of ultrathin nanosheets and ensures the uniform dispersion of cobalt active sites. Moreover, the cationic framework suppresses the competitive HER by electrostatic repulsion between iminium moieties and protons. The resulting iminium-CONs present high activity for six-electron reduction of CO_2 to CH_3OH and exhibit a partial current density of 90.3 mA cm^{-2} with FE_{CH3OH} of 38.7% at −0.74 V using a flow cell. Iminium-CONs are further applied for CO-to-CH_3OH electrochemical conversion and achieve a maximum FE_{CH3OH} of 44.1% at −0.87 V, corresponding to a global FE_{CH3OH} of 54%. The corresponding FE_{H2} is 55.9%, much lower than the 86.6% of pristine CoTAPc at −0.88 V, verifying that HER can be effectively inhibited by cationic iminium-CONs catalyst. Our work provides an effective strategy to enhance the electrocatalytic performance of CO_2 reduction to methanol; while, simultaneously inhibiting hydrogen evolution, accomplished through constructing positively charged covalent organic nanosheets with uniformly distributed cobalt active sites. To the best of our knowledge, this is the first example of ionic covalent organic nanosheets for multielectron reduction of carbon dioxide to methanol.

Supporting Information

Supporting Information is available from the Wiley Online Library or from the author.

Acknowledgements

Y.S., P.G., and T.M. contributed equally to this work. R.Y. acknowledges support from the Guangdong Basic and Applied Basic Research Fund (2022A1515011333), the Hong Kong Research Grant Council (11309723), the Shenzhen Science and Technology Program (JCYJ20220818101204009), and the State Key Laboratory of Marine Pollution (SKLMP/IRF/0029). B.Z.T acknowledges support from the Shenzhen Key Laboratory of Functional Aggregate Materials (ZDSYS20211021111400001) and the Science Technology Innovation Commission of Shenzhen Municipality (KQTD20210811090142053, JCYJ20220818103007014). S.K.R. is thankful for the support from the Strategic Interdisciplinary Research Grant (7020100).

Conflict of Interest

The authors declare no conflict of interest.

Data Availability Statement

The data that support the findings of this study are available from the corresponding author upon reasonable request.

Keywords

carbon dioxide reduction reaction, cationic nanosheets, cobalt phthalocyanine, methanol production, ultrathin nanosheets

Received: September 27, 2023
Revised: October 21, 2023
Published online:

[1] X. Chang, T. Wang, P. Zhang, Y. Wei, J. Zhao, J. Gong, *Angew. Chem., Int. Ed.* **2016**, *128*, 8986.
[2] Z. Jiang, Z. Zhang, H. Li, Y. Tang, Y. Yuan, J. Zao, H. Zheng, Y. Liang, *Adv. Energy Mater.* **2023**, *13*, 2203603.
[3] G. A. Ozin, *Adv. Mater.* **2015**, *27*, 1957.
[4] K. Yang, Y. Sun, S. Chen, M. Li, M. Zheng, L. Ma, W. Fan, Y. Zheng, Q. Li, J. Duan, *Small* **2023**, *19*, 202301536.
[5] C. Hu, Y. Zhang, A. Hu, Y. Wang, X. Wei, K. Shen, L. Chen, Y. Li, *Adv. Mater.* **2023**, *35*, 2209298.
[6] L. Sun, V. Reddu, A. C. Fisher, X. Wang, *Energy Environ. Sci.* **2020**, *13*, 374.
[7] I. E. L. Stephens, K. Chan, A. Bagger, S. W. Boettcher, J. Bonin, E. Boutin, A. K. Buckley, R. Buonsanti, E. R. Cave, X. Chang, S. W. Chee, A. H. M. da Silva, P. de Luna, O. Einsle, B. Endrődi, M. Escudero-Escribano, J. V. Ferreira de Araujo, M. C. Figueiredo, C. Hahn, K. U. Hansen, S. Haussener, S. Hunegnaw, Z. Huo, Y. J. Hwang, C. Janáky, B. S. Jayathilake, F. Jiao, Z. P. Jovanov, P. Karimi, M. T. M. Koper, et al., *J. Phys. Energy* **2022**, *4*, 042003.
[8] X. Liu, B. Q. Li, B. Ni, L. Wang, H. J. Peng, *J. Energy Chem.* **2021**, *64*, 263.
[9] C. Kim, F. Dionigi, V. Beermann, X. Wang, T. Möller, P. Strasser, *Adv. Mater.* **2019**, *31*,1805617.
[10] H. Li, H. Huang, Y. Chen, F. Lai, H. Fu, L. Zhang, N. Zhang, S. Bai, T. Liu, *Adv. Mater.* **2023**, *35*, 2209242.
[11] Y. Li, A. Xu, Y. Lum, X. Wang, S. F. Hung, B. Chen, Z. Wang, Y. Xu, F. Li, J. Abed, J. E. Huang, A. S. Rasouli, J. Wicks, L. K. Sagar, T. Peng, A. H. Ip, D. Sinton, H. Jiang, C. Li, E. H. Sargent, *Nat. Commun.* **2020**, *11*, 6190.
[12] S. S. A. Shah, M. Sufyan Javed, T. Najam, C. Molochas, N. A. Khan, M. A. Nazir, M. Xu, P. Tsiakaras, S. J. Bao, *Coord. Chem. Rev.* **2022**, *471*, 214716.
[13] M. Li, H. Wang, W. Luo, P. C. Sherrell, J. Chen, J. Yang, *Adv. Mater.* **2020**, *32*, 2001848.
[14] H. Yang, Y. Wu, G. Li, Q. Lin, Q. Hu, Q. Zhang, J. Liu, C. He, *J. Am. Chem. Soc.* **2019**, *141*, 12717.
[15] D. H. Nam, O. Shekhah, A. Ozden, C. McCallum, F. Li, X. Wang, Y. Lum, T. Lee, J. Li, J. Wicks, A. Johnston, D. Sinton, M. Eddaoudi, E. H. Sargent, *Adv. Mater.* **2022**, *34*, 207088.

[16] J. D. Yi, D. H. Si, R. Xie, Q. Yin, M. Di Zhang, Q. Wu, G. L. Chai, Y. B. Huang, R. Cao, *Angew. Chem., Int. Ed.* **2021**, *60*, 17108.
[17] Y. Wu, G. Hu, C. L. Rooney, G. W. Brudvig, H. Wang, *ChemSusChem* **2020**, *13*, 6296.
[18] Z. Wang, F. Wang, Y. Peng, Z. Zheng, Y. Han, *Science* **2012**, *338*, 87.
[19] X. Y. Dong, Y. N. Si, Q. Y. Wang, S. Wang, S. Q. Zang, *Adv. Mater.* **2021**, *33*, 2101568.
[20] X. Zhang, Y. Wang, M. Gu, M. Wang, Z. Zhang, W. Pan, Z. Jiang, H. Zheng, M. Lucero, H. Wang, G. E. Sterbinsky, Q. Ma, Y. G. Wang, Z. Feng, J. Li, H. Dai, Y. Liang, *Nat. Energy* **2020**, *5*, 684.
[21] I. Azcarate, C. Costentin, M. Robert, J. M. Savéant, *J. Am. Chem. Soc.* **2016**, *138*, 16639.
[22] S. Dou, L. Sun, S. Xi, X. Li, T. Su, H. J. Fan, X. Wang, *ChemSusChem* **2021**, *14*, 2126.
[23] Y. Song, J. J. Zhang, Y. Dou, Z. Zhu, J. Su, L. Huang, W. Guo, X. Cao, L. Cheng, Z. Zhu, Z. Zhang, X. Zhong, D. Yang, Z. Wang, B. Z. Tang, B. I. Yakobson, R. Ye, *Adv. Mater.* **2022**, *34*, 2110496.
[24] J. Yuan, S. Chen, Y. Zhang, R. Li, J. Zhang, T. Peng, *Adv. Mater.* **2022**, *34*, 2203139.
[25] L. Lin, Q. Zhang, Y. Ni, L. Shang, X. Zhang, Z. Yan, Q. Zhao, J. Chen, *Chem* **2022**, *8*, 1822.
[26] C. S. Diercks, S. Lin, N. Kornienko, E. A. Kapustin, E. M. Nichols, C. Zhu, Y. Zhao, C. J. Chang, O. M. Yaghi, *J. Am. Chem. Soc.* **2018**, *140*, 1116.
[27] M. Zhu, J. Chen, L. Huang, R. Ye, J. Xu, Y. Han, *Angew. Chem., Int. Ed.* **2019**, *131*, 6667.
[28] M. Wang, K. Torbensen, D. Salvatore, S. Ren, D. Joulié, F. Dumoulin, D. Mendoza, B. Lassalle-Kaiser, U. Işci, C. P. Berlinguette, M. Robert, *Nat. Commun.* **2019**, *10*, 3602.
[29] P. Tian, B. Zhang, J. Chen, J. Zhang, L. Huang, R. Ye, B. Bao, M. Zhu, *Catal. Sci. Technol.* **2021**, *11*, 2491.
[30] E. Boutin, M. Wang, J. C. Lin, M. Mesnage, D. Mendoza, B. Lassalle-Kaiser, C. Hahn, T. F. Jaramillo, M. Robert, *Angew. Chem., Int. Ed.* **2019**, *131*, 16318.
[31] S. W. Barr, K. L. Guyer, T. T. T. Li, *J. Electrochem. Soc.* **1984**, *131*, 1511.
[32] Y. Wu, Z. Jiang, X. Lu, Y. Liang, H. Wang, *Nature* **2019**, *575*, 639.
[33] A. K. Ummireddi, S. K. Sharma, R. G. S. Pala, *J. Catal.* **2022**, *406*, 213.
[34] S. Banerjee, C. S. Gerke, V. S. Thoi, *Acc. Chem. Res.* **2022**, *55*, 504.
[35] J. T. Feaster, A. L. Jongerius, X. Liu, M. Urushihara, S. A. Nitopi, C. Hahn, K. Chan, J. K. Nørskov, T. F. Jaramillo, *Langmuir* **2017**, *33*, 9464.
[36] A. K. Ummireddi, S. K. Sharma, R. G. S. Pala, *Catal. Sci. Technol.* **2022**, *12*, 519.
[37] Y. Zhong, Y. Xu, J. Ma, C. Wang, S. Sheng, C. Cheng, M. Li, L. Han, L. Zhou, Z. Cai, Y. Kuang, Z. Liang, X. Sun, *Angew. Chem., Int. Ed.* **2020**, *59*, 19095.
[38] X. Zhang, H. Liu, P. An, Y. Shi, J. Han, Z. Yang, C. Long, J. Guo, S. Zhao, K. Zhao, H. Yin, L. Zheng, B. Zhang, X. Liu, L. Zhang, G. Li, Z. Tang, *Sci. Adv.* **2020**, *6*, eaaz4824.
[39] A. R. Santos, R. K. Blundell, P. Licence, *Phys. Chem. Chem. Phys.* **2015**, *17*, 11839.
[40] N. Mohanapriya, N. Chandrasekaran, *Langmuir* **2022**, *38*, 12581.
[41] J. F. Moulder, W. F. Stickle, P. E. ' Sobol, K. D. Bomben, J. Chastain, *Tech. News - Perkin-Elmer Corp., Opt. Group* **1992**, *40*, 221.
[42] S. Yang, Y. Yu, M. Dou, Z. Zhang, F. Wang, *J. Am. Chem. Soc.* **2020**, *142*, 17524.
[43] J. Su, J. J. Zhang, J. Chen, Y. Song, L. Huang, M. Zhu, B. I. Yakobson, B. Z. Tang, R. Ye, *Energy Environ. Sci.* **2021**, *14*, 483.
[44] F. Dumoulin, M. Durmuş, V. Ahsen, T. Nyokong, *Coord. Chem. Rev.* **2010**, *254*, 2792.
[45] R. Wang, E. Boutin, N. Barreau, F. Odobel, J. Bonin, M. Robert, *ChemPhotoChem* **2021**, *5*, 705.
[46] J. Gu, S. Liu, W. Ni, W. Ren, S. Haussener, X. Hu, *Nat. Catal.* **2022**, *5*, 268.
[47] F. Jia, X. Yu, L. Zhang, *J. Power Sources* **2014**, *252*, 8
[48] J. Huang, Q. Hu, X. Guo, Q. Zeng, L. Wang, *Green Chem.* **2018**, *20*, 2967.
[49] J. Huang, X. Guo, G. Yue, Q. Hu, L. Wang, *ACS Appl. Mater. Interfaces* **2018**, *10*, 44403.
[50] J. Albo, A. Sáez, J. Solla-Gullón, V. Montiel, A. Irabien, *Appl. Catal., B* **2015**, *176*, 709.
[51] S. Payra, S. Shenoy, C. Chakraborty, K. Tarafder, S. Roy, *ACS Appl. Mater. Interfaces* **2020**, *12*, 19402.
[52] Q. Zhang, J. Du, A. He, Z. Liu, C. Tao, *J. CO2 Util.* **2019**, *34*, 635.
[53] X. Sun, Q. Zhu, X. Kang, H. Liu, Q. Qian, Z. Zhang, B. Han, *Angew. Chem., Int. Ed.* **2016**, *55*, 6771.
[54] L. Wang, Y. Xu, T. Chen, D. Wei, X. Guo, L. Peng, N. Xue, Y. Zhu, M. Ding, W. Ding, *J. Catal.* **2021**, *393*, 83.
[55] H. P. Yang, S. Qin, Y. N. Yue, L. Liu, H. Wang, J. X. Lu, *Catal. Sci. Technol.* **2016**, *6*, 6490.
[56] Z. Liang, J. Wang, P. Tang, W. Tang, L. Liu, M. Shakouri, X. Wang, J. Llorca, S. Zhao, M. Heggen, R. E. Dunin-Borkowski, A. Cabot, H. Bin Wu, J. Arbiol, *Appl. Catal., B* **2022**, *314*, 121451.
[57] J. Albo, D. Vallejo, G. Beobide, O. Castillo, P. Castaño, A. Irabien, *ChemSusChem* **2017**, *10*, 1100.
[58] S. Kong, X. Lv, X. Wang, Z. Liu, Z. Li, B. Jia, D. Sun, C. Yang, L. Liu, A. Guan, J. Wang, G. Zheng, F. Huang, *Nat. Catal.* **2023**, *6*, 6.
[59] J. Albo, M. Perfecto-Irigaray, G. Beobide, A. Irabien, *J. CO2 Util.* **2019**, *33*, 157.
[60] J. Liu, D. Yang, Y. Zhou, G. Zhang, G. Xing, Y. Liu, Y. Ma, O. Terasaki, S. Yang, L. Chen, *Angew. Chem., Int. Ed.* **2021**, *60*, 14473.
[61] D. Yang, Q. Zhu, C. Chen, H. Liu, Z. Liu, Z. Zhao, X. Zhang, S. Liu, B. Han, *Nat. Commun.* **2019**, *10*, 667.
[62] J. Su, C. B. Musgrave, Y. Song, L. Huang, Y. Liu, G. Li, Y. Xin, P. Xiong, M. M. J. Li, H. Wu, M. Zhu, H. M. Chen, J. Zhang, H. Shen, B. Z. Tang, M. Robert, W. A. Goddard, R. Ye, *Nat. Catal.* **2023**, *6*, 818.